

Many-Body Coherence in Quantum Transport

Ching-Chi Hang¹ and Liang-Yan Hsu^{1,2,3,*}

¹*Institute of Atomic and Molecular Sciences, Academia Sinica, Taipei, Taiwan*

²*Department of Chemistry, National Taiwan University, Taipei, Taiwan*

³*National Center for Theoretical Sciences, Taipei, Taiwan*

In this study, we propose the concept of harnessing quantum coherence to control electron transport in a many-body system. Combining an open quantum system technique based on Hubbard operators, we show that many-body coherence can eliminate the well-known Coulomb staircase and cause strong negative differential resistance. To explore the mechanism, we analytically derive the current-coherence relationship in the zero electron-phonon coupling limit. Furthermore, by incorporating a gate field, we demonstrate the possibility of constructing a coherence-controlled transistor. This development opens up a new direction for exploring quantum electronic devices based on many-body coherence.

Introduction.— Quantum coherence is a fundamental concept in quantum mechanics that sets it apart from classical physics. The unique properties of quantum coherence have been applied in a diverse range of fields across various disciplines. For instance, quantum coherence has been utilized to enhance the energy transfer efficiency in quantum biology [1–4] and the performance of nanoscale heat engines in quantum thermodynamics [5–9]. Moreover, quantum coherence can be exploited to store and transfer information for quantum communication [10–13]. In nanoelectronics, the importance of quantum coherence is manifested in the interference of a single electron passing through a junction with multiple tunneling pathways, e.g., a quantum interference transistor [14–19]. Despite extensive studies on quantum interference in quantum transport, how to directly connect quantum coherence and transport properties, particularly in many-body systems, remains an open question.

Many-body effects in quantum transport have attracted considerable attention due to their critical significance in open quantum systems and their potential applications in nanoelectronics [20–26]. Numerous intriguing many-body quantum transport phenomena, including Coulomb blockade [27, 28], Kondo resonance [29, 30], Franck-Condon blockade [31–33],

and current hysteresis [34, 35], have been extensively explored in semiconductor nanostructures, 2D materials, and single-molecule junctions. However, the concept of many-body coherence, which refers to quantum coherence between two many-body states, has not received enough attention in the field of quantum transport. In this Letter, we introduce quantum coherence from a Redfield-type fermionic quantum master equation and study quantum transport in a minimal model that incorporates many-body effects such as electron-electron and electron-phonon interactions. Based on this minimal model, we aim to clarify the role of many-body coherence in quantum transport, thus shedding light on how to harness many-body coherence to design quantum electronic devices.

Model Hamiltonian.— To demonstrate the effect of many-body coherence on quantum transport, we consider a quantum electronic device shown in Fig. 1. The device is described by the total Hamiltonian $\hat{H} = \hat{H}_{\text{sys}} + \hat{H}_{\text{lead}} + \hat{H}_{\text{sys-lead}} + \hat{H}_{\text{gate}}$ composed of the system Hamiltonian \hat{H}_{sys} , the lead Hamiltonian \hat{H}_{lead} , the system-lead coupling term $\hat{H}_{\text{sys-lead}}$, and the gate Hamiltonian \hat{H}_{gate} . Furthermore, to simplify the complexity of a many-body system without loss of generality, we consider the two-site Peierls–Hubbard model [36, 37] to be the system, including on-site energy ε , on-site Coulomb repulsion U , intersite electron hopping t and electron-phonon coupling strength g .

For the convenience of theoretical analysis, we rearrange the terms in the two-site Peierls–Hubbard model as $\hat{H}_{\text{sys}} = \hat{H}_{\text{el}} + \hat{H}_{\text{ph}} + \hat{H}_{\text{el-ph}}$ composed of the electronic Hamiltonian \hat{H}_{el} , the phonon Hamiltonian \hat{H}_{ph} , and the electron-phonon coupling $\hat{H}_{\text{el-ph}}$. The electronic Hamiltonian has the form $\hat{H}_{\text{el}} = \varepsilon \sum_{i,\sigma} \hat{c}_{i\sigma}^\dagger \hat{c}_{i\sigma} + U \sum_i \hat{c}_{i\uparrow}^\dagger \hat{c}_{i\uparrow} \hat{c}_{i\downarrow}^\dagger \hat{c}_{i\downarrow} - t \sum_{\sigma} (\hat{c}_{2\sigma}^\dagger \hat{c}_{1\sigma} + \text{H.c.})$, where $\hat{c}_{i\sigma}^\dagger$ ($\hat{c}_{i\sigma}$) is the fermionic operator which creates (annihilates) an electron on site $i = 1, 2$ with spin $\sigma = \uparrow, \downarrow$. The model can accommodate at most 4 electrons and generate 16 different many-body electronic states in total [38]. To properly describe many-body states, we denote the many-body states of the system as $|N_a, a\rangle$ with energy ε_a as shown in Table I, where N_a represents the number of electrons of state a . We consider the phonon Hamiltonian $\hat{H}_{\text{ph}} = \sum_{\alpha} \hbar \omega_{\alpha} (\hat{b}_{\alpha}^\dagger \hat{b}_{\alpha} + \frac{1}{2})$ and the electron-phonon coupling

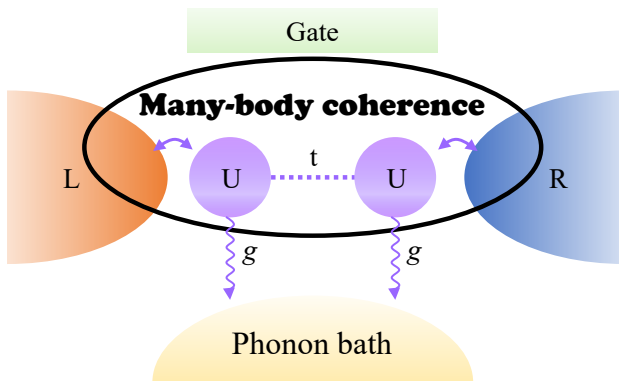


FIG. 1. Illustration of a quantum electronic device in a many-body system. The system coupled with one gate and two leads L and R contains on-site Coulomb repulsion U , intersite electron hopping t , and electron-phonon coupling g .

$\hat{H}_{\text{el-ph}} = g \sum_{i,\sigma,\alpha} \hat{c}_{i\sigma}^\dagger \hat{c}_{i\sigma} (\hat{b}_\alpha^\dagger + \hat{b}_\alpha)$, where ω_α and \hat{b}_α^\dagger (\hat{b}_α) stand for phonon frequency and bosonic creation (annihilation) operator of the phonon mode α , respectively. According to the previous study [39], we believe that a two-site system, such as thiolated arylethynylene with 9,10-dihydroanthracene core (AH), is experimentally feasible for the demonstration of the effect of many-body coherence on quantum transport.

The two leads and the gate are modeled as follows. For the gate, we model its Hamiltonian as $\hat{H}_{\text{gate}} = -eV_g \sum_{i,\sigma} \hat{c}_{i\sigma}^\dagger \hat{c}_{i\sigma}$, where the gate voltage V_g shifts the on-site energy ε by $-eV_g$. The two leads are described by a noninteracting electron gas model, $\hat{H}_{\text{lead}} = \sum_{l,k,\sigma} \xi_{k\sigma} \hat{d}_{lk\sigma}^\dagger \hat{d}_{lk\sigma}$, where $\hat{d}_{lk\sigma}^\dagger$ ($\hat{d}_{lk\sigma}$) creates (annihilates) an electron in the state $|lk\sigma\rangle$ with energy $\xi_{lk\sigma}$ in the lead l , and $l = \text{L}$ and R represents the left and the right leads. Assuming that the electrons in the leads stay at equilibrium, we express the average occupation number as $\langle \hat{d}_{lk\sigma}^\dagger \hat{d}_{lk'\sigma'} \rangle = \delta_{l,l'} \delta_{k,k'} \delta_{\sigma,\sigma'} f_l(\xi_{k\sigma})$, where $f_l(\xi_{k\sigma}) = (1 + e^{(\xi_{k\sigma} - \mu_l)/k_B T})^{-1}$ is the Fermi function of lead l with chemical potential μ_l at temperature T . In this work, we consider the symmetric bias condition $\mu_l = \mu_0 + \zeta_l eV_{\text{sd}}/2$ with $\zeta_{\text{L}} = 1$ and $\zeta_{\text{R}} = -1$, where V_{sd} is the bias voltage, and μ_0 is the equilibrium chemical potential for the electrodes. The system-lead coupling is modeled as $\hat{H}_{\text{sys-lead}} = \sum_{k,\sigma} (T_{\text{L}k,1} \hat{c}_{1\sigma}^\dagger \hat{d}_{\text{L}k\sigma} + T_{\text{R}k,2} \hat{c}_{2\sigma}^\dagger \hat{d}_{\text{R}k\sigma} + \text{H.c.})$, where we assume the left (right) lead is only coupled to the first (second) site of the system. Furthermore, we specify the transitions between many-body states using Hubbard operators $\hat{X}^{a,b} \equiv |N_a, a\rangle \langle N_b, b|$ (see Supplemental Material [40] for more details). The advantage of using Hubbard operators is to provide a convenient way to describe many-body state transitions and incorporate characteristics of fermions in the coefficient of each operator [38, 41]. As a result, we rewrite the coupling Hamiltonian as $\hat{H}_{\text{sys-lead}} = \sum_{ab,k,\sigma} (V_{\text{L}k\sigma,ab}^* \hat{X}^{b,a} \hat{d}_{\text{L}k\sigma} + V_{\text{R}k\sigma,ab}^* \hat{X}^{b,a} \hat{d}_{\text{R}k\sigma} + \text{H.c.})$ based on the Hubbard operator techniques, where the transformed coupling becomes $V_{\text{L}k\sigma,ab} = T_{\text{L}k,i}^* \cdot \langle N_a, a | \hat{c}_{i\sigma} | N_b, b \rangle$. The index i is neglected in $V_{\text{L}k\sigma,ab}$ because i is uniquely determined by l , i.e., $i = 1$ (2) when $l = \text{L}$ (R). Note that, for simplicity, we ignore the external potential exerted by the bias on the system, i.e., the on-site energy ε does not vary with the source-drain voltage V_{sd} .

Quantum master equation analysis.— To incorporate the effect of many-body coherence into quantum transport, instead of using the Pauli master equation (PME) or the Lindblad quantum master equation, we adopt the Redfield formalism, which has been used extensively to describe phonon effects on quantum transport [43–46], for treating electronic bath in the electrodes and phonon bath together. We start from the quantum Liouville equation, treat the two leads \hat{H}_{lead} and phonons \hat{H}_{ph} as bath, make the Born-Markov approximation, and finally derive a Redfield-type fermionic quantum master equation based on Hubbard operators (see Supplemental Material [40] for more details) as follows,

$$\frac{d\hat{\rho}_{\text{el}}(t)}{dt} = -\frac{i}{\hbar} [\hat{H}_{\text{el}}, \hat{\rho}_{\text{el}}(t)] + \mathcal{R}_{\text{lead}} \hat{\rho}_{\text{el}}(t) + \mathcal{R}_{\text{ph}} \hat{\rho}_{\text{el}}(t), \quad (1)$$

where $\mathcal{R}_{\text{lead}}$ is the lead Redfield superoperator which de-

Hilbert space	Energy ε_a	Eigenstate $ N_a, a\rangle$
Zero-electron	0	$ 0, S^0\rangle$
One-electron	$\varepsilon - t$	$ 1, D_{+, \uparrow}^1\rangle, 1, D_{-, \downarrow}^1\rangle$
	$\varepsilon + t$	$ 1, D_{-, \uparrow}^1\rangle, 1, D_{-, \downarrow}^1\rangle$
Two-electron	$2\varepsilon - (x - U)/2$	$ 2, S_+^2\rangle$
	2ε	$ 2, T_0^2\rangle, 2, T_{+1}^2\rangle, 2, T_{-1}^2\rangle$
	$2\varepsilon + U$	$ 2, S_{\text{CS}}^2\rangle$
	$2\varepsilon + (x + U)/2$	$ 2, S_-^2\rangle$
Three-electron	$3\varepsilon + U - t$	$ 3, D_{-, \uparrow}^3\rangle, 3, D_{-, \downarrow}^3\rangle$
	$3\varepsilon + U + t$	$ 3, D_{+, \uparrow}^3\rangle, 3, D_{+, \downarrow}^3\rangle$
Four-electron	$4\varepsilon + 2U$	$ 4, S^4\rangle$

TABLE I. The 16 eigenstates of the system Hamiltonian and their corresponding energies [42], $x \equiv \sqrt{U^2 + 16t^2}$.

scribes the electron transport processes between the system and electrodes, \mathcal{R}_{ph} is the phonon Redfield superoperator which accounts for the influence of phonons on electrons in the system, and $\hat{\rho}_{\text{el}}(t)$ is the electronic density matrix. In order to focus on many-body electronic coherence and perform an analytical analysis, we neglect the effect of $\mathcal{R}_{\text{ph}} \hat{\rho}_{\text{el}}(t)$ in the main text and leave the discussion about the effects of phonons on coherence and transport properties in the Supplemental Material [40].

Specifically, the operation of the lead Redfield superoperator on the electronic density matrix can be expressed as

$$\begin{aligned} \mathcal{R}_{\text{lead}} \hat{\rho}_{\text{el}}(t) = & -\frac{i}{\hbar} \sum_{abcd} \sum_l \left\{ \begin{aligned} & \left[\Sigma_{db,ca}^{(l),<}(\varepsilon_{bd}) - \left(\Sigma_{ca,db}^{(l),<}(\varepsilon_{ac}) \right)^* \right] \rho_{cd} \\ & + \left[-\Sigma_{bd,ac}^{(l),>}(\varepsilon_{ca}) + \left(\Sigma_{ac,bd}^{(l),>}(\varepsilon_{db}) \right)^* \right] \rho_{cd} \\ & - \left[-\Sigma_{da,dc}^{(l),>}(\varepsilon_{cd}) - \left(\Sigma_{cd,ad}^{(l),<}(\varepsilon_{dc}) \right)^* \right] \rho_{cb} \\ & - \left[\Sigma_{cd,bd}^{(l),<}(\varepsilon_{dc}) + \left(\Sigma_{db,dc}^{(l),>}(\varepsilon_{cd}) \right)^* \right] \rho_{ac} \end{aligned} \right\} \hat{X}^{a,b} \quad (2) \end{aligned}$$

where states (a, b, c, d) serve as the eigenstates of \hat{H}_{el} , and $\varepsilon_{ab} = \varepsilon_a - \varepsilon_b$ is the energy difference between state $|N_a, a\rangle$ and $|N_b, b\rangle$. The lesser (greater) self-energy $\Sigma_{ca,db}^{(l),<} (\Sigma_{ca,db}^{(l),>})$ is associated with the state transitions $|N_c, c\rangle \leftrightarrow |N_a, a\rangle$ and $|N_d, d\rangle \leftrightarrow |N_b, b\rangle$ regarding one electron (hole) injection from the leads. Note that the order of the subscript of the self-energy represents the transition from the N -electron state to the $(N+1)$ -electron state, e.g., $\Sigma_{ca,db}^{(l),<}$ describes state transitions $|N_c = N, c\rangle \rightarrow |N_a = N+1, a\rangle$ and $|N_d = N, d\rangle \rightarrow |N_b = N+1, b\rangle$ regarding one electron injection from the

leads. The self-energy terms can be expressed as [41]

$$\begin{aligned}\Sigma_{ca,db}^{(l),<}(\epsilon_{ac}) &= \sum_{k,\sigma} V_{lk\sigma,ca}^* g_{lk\sigma}^{<}(\epsilon_{ac}) V_{lk\sigma,db} \\ \Sigma_{ca,db}^{(l),>}(\epsilon_{ac}) &= \sum_{k,\sigma} V_{lk\sigma,ca}^* g_{lk\sigma}^{>}(\epsilon_{ac}) V_{lk\sigma,db},\end{aligned}$$

where the lesser (greater) Green's function of electrons $g_{lk\sigma}^{<}(\epsilon_{ac})$ ($g_{lk\sigma}^{>}(\epsilon_{ac})$) contains the occupation of electrons (holes) in the leads. For simplicity, we consider the wideband approximation, and the lesser self-energy can be simplified as

$$\begin{aligned}\Sigma_{ca,db}^{(l),<}(\epsilon_{ac}) &= i \frac{\Gamma}{2} f_l(\epsilon_{ac}) \times \\ &\sum_{\sigma} [\langle N_a, a | \hat{c}_{i\sigma}^\dagger | N_c, c \rangle]^* \langle N_b, b | \hat{c}_{i\sigma}^\dagger | N_d, d \rangle, \quad (3)\end{aligned}$$

which is composed of a coupling constant Γ , the occupation of electrons $f_l(\epsilon_{ac})$, and the transition amplitude between many-body states of the system due to an injected electron $\Sigma_{\sigma} [\langle N_a, a | \hat{c}_{i\sigma}^\dagger | N_c, c \rangle]^* \langle N_b, b | \hat{c}_{i\sigma}^\dagger | N_d, d \rangle$. Similarly, the greater self-energy in the wideband approximation comprises a coupling constant Γ , the occupation of holes $1 - f_l(\epsilon_{ac})$, and the transition amplitude between many-body states of the system due to a hole entering the system.

To explore the correlation between the steady-state electric current and many-body coherence, we compute the electric current [47] from the steady-state density matrix $\hat{\rho}_{\text{el}}(t)$ as

$$I = \frac{2e}{\hbar} \sum_{acd} \text{Im} \left\{ \left[\Sigma_{da,ca}^{(\text{L}),<}(\epsilon_{ad}) - \left(\Sigma_{ac,ad}^{(\text{L}),>}(\epsilon_{da}) \right)^* \right] \rho_{cd} \right\}, \quad (4)$$

where $\Sigma_{da,ca}^{(\text{L}),<}(\epsilon_{ad})$ corresponds to a transition from N -electron to $(N+1)$ -electron state due to an injected electron from the left electrode, while $\Sigma_{ac,ad}^{(\text{L}),>}(\epsilon_{da})$ corresponds to a transition from N -electron to $(N-1)$ -electron state caused by an injected hole.

Many-body coherence and current blockade.— To demonstrate that the effect of many-body coherence on quantum transport can be experimentally observed in a realistic system, we consider AH with experimental parameters [39]. As shown in Fig. 2a, the electric current (the black solid line) decreases as many-body coherence between eigenstates $|2, S_{\text{CS}}^2\rangle$ and $|2, S_-^2\rangle$ (the blue dashed line) increases with bias. Furthermore, we find that, for a model system with large Coulomb repulsion and weak intersite electron hopping, many-body coherence can reach a maximum, and the electric current can be completely blocked to zero, as shown in Fig. 2b. It is worth mentioning that the current blockade phenomenon in Fig. 2a and 2b is completely different from the well-known “Coulomb blockade”. In Coulomb blockade, the electric current exhibits “Coulomb staircase” with the increasing bias voltage (the orange solid lines in Fig. 2a and 2b), whereas Fig. 2a and 2b show that the electric current decreases with the increasing bias voltage, similar to the behavior of a negative difference resistance. Here, we would like to emphasize that Coulomb staircase can be fully understood by the

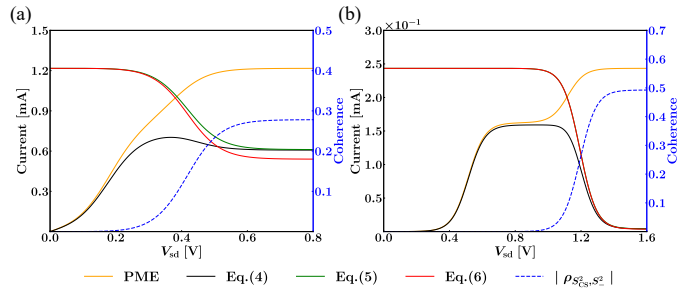


FIG. 2. Current blockade induced by many-body coherence in an AH system [39] for (a) $\epsilon = 0.1$ eV, $t = 0.01$ eV, $U = 0.08$ eV, $\Gamma = 0.005$ eV and in a model system for (b) $\epsilon = -0.25$ eV, $t = 0.005$ eV, $U = 0.8$ eV, $\Gamma = 0.001$ eV. Other parameters are $T = 300$ K, $V_g = 0$ V, and $g = 0$ (no electron-phonon coupling). The cases for $g \neq 0$ can be found in Supplemental Material [40]. The orange, black, green, and red solid lines correspond to steady-state currents derived from PME, Eq. (4), Eq. (5), and Eq. (6), respectively. The dashed blue line describes the magnitude of coherence $|\rho_{S_{\text{CS}}^2, S_-^2}|$.

PME approach, and this approach is extensively employed to study nanodevices [42, 48, 49]. However, the PME approach does not account for the effect of “coherence” induced by the interaction between many-body states and electron baths. Note that the current suppression is found to be robust against electron-phonon couplings when g is not large (see Supplemental Material [40] for more details). Our numerical simulations clearly demonstrate that coherence between many-body states cannot be neglected and is directly associated with electric current.

To quantitatively understand the current blockade in Fig. 2a and 2b, we derive a current-coherence relationship for a system with weak hopping and strong Coulomb repulsion. The relationship is established based on two assumptions. First, to include the effect of Coulomb repulsion U on currents, we consider that $eV_{\text{sd}} > U$ in the zero temperature limit. Furthermore, for the simplicity of derivation, we neglect the influence of ϵ and t on the Fermi function. In this condition, we can approximate $f_L(\epsilon_{ac}) = 1$ and $f_R(\epsilon_{ac}) = 0$ in Eq. (3). Second, we only keep many-body coherence $\rho_{S_+^2, T_0^2}$, $\rho_{S_+^2, T_{+1}^2}$, $\rho_{S_+^2, T_{-1}^2}$ and $\rho_{S_{\text{CS}}^2, S_-^2}$ when solving Eq. (1). It is well-known that coherence can be neglected while there is a large energy gap between two states, i.e., the secular approximation for the derivation of the PME approach. When t/U is small, the energy gap between $|2, S_{\text{CS}}^2\rangle$ and $|2, S_-^2\rangle$ and the energy gap between $|2, S_+^2\rangle$ and triplet states $|2, T_0^2\rangle$, $|2, T_{+1}^2\rangle$, $|2, T_{-1}^2\rangle$ are the smallest. As a result, we consider these coherence terms when solving Eq. (1) and find that only $\rho_{S_{\text{CS}}^2, S_-^2}$ is associated with current. Finally, we obtain a current-coherence relationship as (see Supplemental Material [40] for more details)

$$I = \frac{e\Gamma}{\hbar} \left\{ 1 - 2 \left[1 + \frac{1}{4} \left(\frac{4t^2}{U\Gamma} \right)^2 \right]^{-1/2} \left| \rho_{S_{\text{CS}}^2, S_-^2} \right| \right\}, \quad (5)$$

showing that the electric current can be expressed in terms of many-body coherence $\rho_{S_{\text{CS}}^2, S_-^2}$ and the kinetic exchange

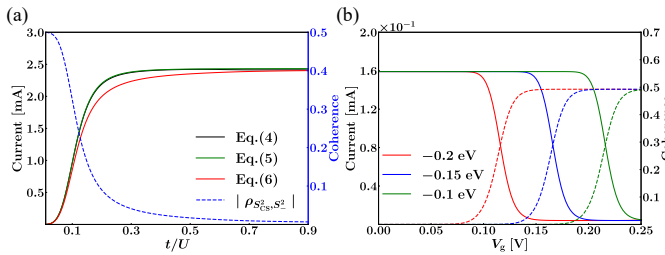


FIG. 3. Coherence-controlled current blockade of a model system tuned by (a) the Hamiltonian design t/U for $\varepsilon = -0.1$ eV, $t = 0.002$ to 0.18 eV, $U = 0.2$ eV, $\Gamma = 0.01$ eV under bias $V_{sd} = 0.8$ V, gate $V_g = 0$ V and (b) the gate voltage V_g for $t = 0.005$ eV, $U = 0.8$ eV, $\Gamma = 0.001$ eV under bias $V_{sd} = 1.0$ V, gate $V_g = 0.1$ to 0.35 V. The black, green, and red solid lines in (a) correspond to currents from Eq. (4), Eq. (5), and Eq. (6), and the dashed blue line denotes the magnitude of coherence $|\rho_{S_{CS}^2, S_{-}^2}|$. The red, blue, and green lines in (b) correspond to $\varepsilon = -0.2, -0.15, -0.1$ eV, and the solid and dashed lines denote currents and the magnitude of coherence $|\rho_{S_{CS}^2, S_{-}^2}|$ respectively. Other parameters used here are $g = 0$ (no electron-phonon coupling), $T = 300$ K for (a) and $T = 77$ K for (b).

$4t^2/U$ in the unit of system-lead coupling Γ . In Fig. 2a and 2b, the green lines almost coincide with the black lines when current blockade occurs, which reveals that Eq. (5) has successfully captured the physics behind the current blockade and elucidated the influence of many-body coherence on quantum transport. Furthermore, the kinetic exchange $4t^2/U$, resulting from the interplay between hopping and many-body interactions, describes the intersite delocalization of electrons. Therefore, when the kinetic exchange is small, electrons accumulate on a single site, and the current is blockaded. Note that $4t^2/U$ corresponds to the energy gap $\Delta E_{S_{CS}^2, S_{-}^2} = (\sqrt{U^2 + 16t^2} - U)/2$ when $t/U \ll 1$. If the energy gap $\Delta E_{S_{CS}^2, S_{-}^2}$ is small enough, i.e., $4t^2/UT\Gamma$ is negligible, then Eq. (5) can be further simplified as

$$I = \frac{e\Gamma}{\hbar} \left\{ 1 - 2|\rho_{S_{CS}^2, S_{-}^2}| \right\}, \quad (6)$$

indicating that many-body coherence $\rho_{S_{CS}^2, S_{-}^2}$ becomes a dominant factor in current blockade. When t/U is not small enough, e.g., $t/U = 0.125$ in Fig. 2a, Eq. (6) (the red line) slightly underestimates the electric current in the current blockade region due to the neglect of the kinetic exchange effect. On the other hand, when $t/U \ll 1$, e.g., $t/U = 0.00625$ in Fig. 2b, the red line matches the black line in the current blockade region, testifying that many-body coherence predominates the current suppression.

Control of current blockade.— Control of electric current is a key issue in quantum transport [16, 50–53]. Here, we demonstrate that it is feasible to operate many-body coherence and current blockade via internal Hamiltonian design and an external gate voltage.

First, for Hamiltonian design, the relative magnitudes of intersite coupling t and Coulomb repulsion U are directly related to many-body coherence and current blockade. As

shown in Fig. 3a, when $t/U \ll 0.1$, the current decreases to almost zero, and many-body coherence $\rho_{S_{CS}^2, S_{-}^2}$ approaches its maximum 0.5. In brief, the maximum value of coherence can be understood by the fact that small t/U reduces the energy gap between $|2, S_{CS}^2\rangle$ and $|2, S_{-}^2\rangle$ to almost zero and thus leads to the maximum of $\rho_{S_{CS}^2, S_{-}^2} = 0.5$. The origin of strong current blockade results mainly from many-body coherence $\rho_{S_{CS}^2, S_{-}^2}$, i.e., when $t/U \ll 0.1$, the current calculated from Eq. (6) (the red line), which neglects the kinetic exchange effect, coincides with the current calculated from Eq. (5) (the green line). The small deviation between the green line and the red line in the region $t/U \approx 0.1 \sim 0.7$ indicates that the kinetic exchange $4t^2/U$ can affect the electric current, but many-body coherence is still the main mechanism for the current blockade. When $t/U \gg 0.7$, many-body coherence $\rho_{S_{CS}^2, S_{-}^2}$ reaches zero, so current blockade disappears. Fig. 3a clearly shows that one can control electric current and many-body coherence via the modification of t/U .

Second, we find that many-body coherence of a system can be significantly influenced by an external gate field. Fig. 3b shows that, with an increasing gate voltage V_g , many-body coherence $\rho_{S_{CS}^2, S_{-}^2}$ transitions from zero to its maximum and the current drops to zero. Moreover, the transition gate voltage increases with the increasing on-site energy ε , where the red, blue, and green line correspond to $\varepsilon = -0.2, -0.15$, and -0.1 eV, respectively. Control of the gate voltage V_g and the Hamiltonian design correspond to different mechanisms of forming the current blockade because control of V_g does not change the kinetic exchange $4t^2/U$. To explain the gate dependence of many-body coherence $\rho_{S_{CS}^2, S_{-}^2}$, we derive an analytical expression for the coherence-gate relationship, $|\rho_{S_{CS}^2, S_{-}^2}| = 1/2 \times [2 - \Theta(\mu_L - \varepsilon - U + eV_g)] / [8 - 7\Theta(\mu_L - \varepsilon - U + eV_g)]$, by making the approximation $f_L(\varepsilon + U - eV_g) = \Theta(\mu_L - \varepsilon - U + eV_g)$ and $t \approx 0$ (see Supplemental Material [40] for more details), where $\Theta(\mu_L - \varepsilon - U + eV_g)$ is the Heaviside step function. According to the coherence-gate relation, when $\varepsilon = -0.2$ eV, $U = 0.8$ eV, and $V_{sd} = 1.0$ V, many-body coherence $\rho_{S_{CS}^2, S_{-}^2}$ has a maximum value 0.5 while V_g exceeds 0.1 V, which is consistent with our simulation result (the red line). Fig. 3b also indicates that, with lower on-site energies, the electric current and many-body coherence can be operated with smaller gate voltages, showing potential as transistors.

Conclusions.— We have demonstrated the significance of many-body coherence in quantum transport and established a current-coherence relationship Eq. (5) for a model system using the Redfield-type fermionic quantum master equation. The results imply that many-body coherence can eliminate the well-known Coulomb staircase and lead to strong negative differential resistance, which cannot be described by the PME approach [42, 48, 49] due to the lack of coherence. Furthermore, it is shown that many-body coherence can be manipulated through modifying the internal system Hamiltonian or applying an external gate voltage. Finally, we find that the electric current can be switched based on many-body coherence.

ence at a low gate voltage, indicating potential as coherence-controlled transistors. The results here open a new class of electronic devices in quantum electronics, which will motive further experimental and theoretical investigations on the effects of many-body coherence in condensed matter physics and quantum technology.

We thank Chih-En Shen, Hung-Sheng Tsai, Ming-Wei Lee, Yi-Ting Chuang, Qian-Rui Huang, Michitoshi Hayashi, and Yang-Hao Chan for useful discussions. This research was supported by the Academia Sinica (AS-CDA-111-M02) and the Ministry of Science and Technology of Taiwan (Grant Nos. 110-2113-M-001-053 and 111-2113-M-001-027-MY4).

* lyhsu@gate.sinica.edu.tw

- [1] G. S. Engel, T. R. Calhoun, E. L. Read, T.-K. Ahn, T. Mančal, Y.-C. Cheng, R. E. Blankenship, and G. R. Fleming, *Nature (London)* **446**, 782 (2007).
- [2] G. Panitchayangkoon, D. Hayes, K. A. Fransted, J. R. Caram, E. Harel, J. Wen, R. E. Blankenship, and G. S. Engel, *Proc. Natl. Acad. Sci. U.S.A.* **107**, 12766 (2010).
- [3] G. D. Scholes, G. R. Fleming, L. X. Chen, A. Aspuru-Guzik, A. Buchleitner, D. F. Coker, G. S. Engel, R. van Grondelle, A. Ishizaki, and D. M. Jonas *et al.*, *Nature (London)* **543**, 647 (2017).
- [4] J.-L. Brédas, E. H. Sargent, and G. D. Scholes, *Nat. Mater.* **16**, 35 (2017).
- [5] M. O. Scully, K. R. Chapin, K. E. Dorfman, M. B. Kim, and A. Svidzinsky, *Proc. Natl. Acad. Sci. U.S.A.* **108**, 15097 (2011).
- [6] P. Samuelsson, S. Kheradsoud, and B. Sothmann, *Phys. Rev. Lett.* **118**, 256801 (2017).
- [7] S. Saryal, M. Gerry, I. Khait, D. Segal, and B. K. Agarwalla, *Phys. Rev. Lett.* **127**, 190603 (2021).
- [8] H. Tajima and K. Funo, *Phys. Rev. Lett.* **127**, 190604 (2021).
- [9] S. Kamimura, H. Hakoshima, Y. Matsuzaki, K. Yoshida, and Y. Tokura, *Phys. Rev. Lett.* **128**, 180602 (2022).
- [10] K.-D. Wu, Z. Hou, Y.-Y. Zhao, G.-Y. Xiang, C.-F. Li, G.-C. Guo, J. Ma, Q.-Y. He, J. Thompson, and M. Gu, *Phys. Rev. Lett.* **121**, 050401 (2018).
- [11] C. T. Nguyen, D. D. Sukachev, M. K. Bhaskar, B. Machielse, D. S. Levonian, E. N. Knall, P. Stroganov, R. Riedinger, H. Park, and M. Lončar *et al.*, *Phys. Rev. Lett.* **123**, 183602 (2019).
- [12] M. K. Bhaskar, R. Riedinger, B. Machielse, D. S. Levonian, C. T. Nguyen, E. N. Knall, H. Park, D. Englund, M. Lončar, and D. D. Sukachev *et al.*, *Nature (London)* **580**, 60 (2020).
- [13] L. Zhai, G. N. Nguyen, C. Spinnler, J. Ritzmann, M. C. Löbl, A. D. Wieck, A. Ludwig, A. Javadi, and R. J. Warburton, *Nat. Nanotechnol.* **17**, 829 (2022).
- [14] C. M. Guédon, H. Valkenier, T. Markussen, K. S. Thygesen, J. C. Hummelen, and S. J. van der Molen, *Nat. Nanotechnol.* **7**, 305 (2012).
- [15] S. Ballmann, R. Härtle, P. B. Coto, M. Elbing, M. Mayor, M. R. Bryce, M. Thoss, and H. B. Weber, *Phys. Rev. Lett.* **109**, 056801 (2012).
- [16] L.-Y. Hsu and H. Rabitz, *Phys. Rev. Lett.* **109**, 186801 (2012).
- [17] Y. Li, M. Buerkle, G. Li, A. Rostamian, H. Wang, Z. Wang, D. R. Bowler, T. Miyazaki, L. Xiang, and Y. Asai *et al.*, *Nat. Mater.* **18**, 357 (2019).
- [18] J. Bai, A. Daaoub, S. Sangtarash, X. Li, Y. Tang, Q. Zou, H. Sadeghi, S. Liu, X. Huang, and Z. Tan *et al.*, *Nat. Mater.* **18**, 364 (2019).
- [19] J. E. Greenwald, J. Cameron, N. J. Findlay, T. Fu, S. Gunesekaran, P. J. Skabara, and L. Venkataraman, *Nat. Nanotechnol.* **16**, 313 (2021).
- [20] M. Galperin, M. A. Ratner, and A. Nitzan, *J. Phys. Condens. Matter* **19**, 103201 (2007).
- [21] A. K. Mitchell, K. G. L. Pedersen, P. Hedegård, and J. Paaske, *Nat. Commun.* **8**, 15210 (2017).
- [22] P. Yu, N. Kocić, J. Repp, B. Siegert, and A. Donarini, *Phys. Rev. Lett.* **119**, 056801 (2017).
- [23] B. Fu, M. A. Mosquera, G. C. Schatz, M. A. Ratner, and L.-Y. Hsu, *Nano Lett.* **18**, 5015 (2018).
- [24] K. Kimura, K. Miwa, H. Imada, M. Imai-Imada, S. Kawahara, J. Takeya, M. Kawai, M. Galperin, and Y. Kim, *Nature (London)* **570**, 210 (2019).
- [25] J. H. Fetherolf, D. Golež, and T. C. Berkelbach, *Phys. Rev. X* **10**, 021062 (2020).
- [26] O. Shein-Lumbroso, J. Liu, A. Shastry, D. Segal, and O. Tal, *Phys. Rev. Lett.* **128**, 237701 (2022).
- [27] J. Park, A. N. Pasupathy, J. I. Goldsmith, C. Chang, Y. Yalsh, J. R. Petta, M. Rinkoski, J. P. Sethna, H. D. Abruna, P. L. McEuen, and D. C. Ralph, *Nature (London)* **417**, 722 (2002).
- [28] M. Brotons-Gisbert, A. Branny, S. Kumar, R. Picard, R. Proux, M. Gray, K. S. Burch, K. Watanabe, T. Taniguchi, and B. D. Gerardot, *Nat. Nanotechnol.* **14**, 442 (2019).
- [29] W. Liang, M. P. Shores, M. Bockrath, J. R. Long, and H. Park, *Nature (London)* **417**, 725 (2002).
- [30] A. Kurzmann, Y. Kleeorin, C. Tong, R. Garreis, A. Knothe, M. Eich, C. Mittag, C. Gold, F. K. de Vries, and K. Watanabe *et al.*, *Nat. Commun.* **12**, 6004 (2021).
- [31] J. Koch and F. von Oppen, *Phys. Rev. Lett.* **94**, 206804 (2005).
- [32] E. Burzurí, Y. Yamamoto, M. Warnock, X. Zhong, K. Park, A. Cornia, and H. S. Van Der Zant, *Nano Lett.* **14**, 3191 (2014).
- [33] S. Du, Y. Hashikawa, H. Ito, K. Hashimoto, Y. Murata, Y. Hirayama, and K. Hirakawa, *Nano Lett.* **21**, 10346 (2021).
- [34] M. Galperin, M. A. Ratner, and A. Nitzan, *Nano Lett.* **5**, 125 (2005).
- [35] F. Schwarz, G. Kastlunger, F. Lissel, C. Egler-Lucas, S. N. Semenov, K. Venkatesan, H. Berke, R. Stadler, and E. Lörtscher, *Nat. Nanotechnol.* **11**, 170 (2016).
- [36] Y. Toyozawa, *J. Phys. Soc. Japan* **50**, 1861 (1981).
- [37] L.-Y. Hsu, T.-W. Tsai, and B.-Y. Jin, *J. Chem. Phys.* **133**, 144705 (2010).
- [38] B. Li, W. H. Miller, T. J. Levy, and E. Rabani, *J. Chem. Phys.* **140**, 204106 (2014).
- [39] M. Koole, J. C. Hummelen, and H. S. J. van der Zant, *Phys. Rev. B* **94**, 165414 (2016).
- [40] See Supplemental Material at [URL will be inserted by publisher], which includes Refs. [38, 39, 41, 43, 47], for additional details on Hubbard operators, the derivation of the Redfield-type fermionic quantum master equation, phonon effects, and derivations of the current-coherence and the coherence-gate relationship.
- [41] M. Esposito and M. Galperin, *Phys. Rev. B* **79**, 205303 (2009).
- [42] J. O. Thomas, J. K. Sowa, B. Limburg, X. Bian, C. Evangelisti, J. L. Swett, S. Tewari, J. Baugh, G. C. Schatz, and G. A. D. Briggs *et al.*, *Chem. Sci.* **12**, 11121 (2021).
- [43] D. Segal, A. Nitzan, W. B. Davis, M. R. Wasielewski, and M. A. Ratner, *J. Phys. Chem. B* **104**, 3817 (2000).
- [44] L.-Y. Hsu, N. Wu, and H. Rabitz, *J. Phys. Chem. Lett.* **5**, 1831 (2014).
- [45] B. K. Agarwalla, J.-H. Jiang, and D. Segal, *Phys. Rev. B* **92**, 245418 (2015).

- [46] N. Anto-Sztrikacs, A. Nazir, and D. Segal, PRX Quantum **4**, 020307 (2023).
- [47] H. Haug and A.-P. Jauho, *Quantum Kinetics in Transport and Optics of Semiconductors* (Springer, Berlin, Heidelberg, 2008).
- [48] C. J. Boyle, M. Upadhyaya, P. Wang, L. A. Renna, M. Lu-Díaz, S. Pyo Jeong, N. Hight-Huf, L. Korugic-Karasz, M. D. Barnes, and Z. Aksamija *et al.*, Nat. Commun. **10**, 2827 (2019).
- [49] P. B. Vyas, M. L. Van de Put, and M. V. Fischetti, Phys. Rev. Appl. **13**, 014067 (2020).
- [50] M. Grifoni and P. Hänggi, Phys. Rep. **304**, 229 (1998).
- [51] L.-Y. Hsu, E. Y. Li, and H. Rabitz, Nano Lett. **13**, 5020 (2013).
- [52] A. J. White, U. Peskin, and M. Galperin, Phys. Rev. B **88**, 205424 (2013).
- [53] F. Damanet, E. Mascarenhas, D. Pekker, and A. J. Daley, Phys. Rev. Lett. **123**, 180402 (2019).